

***GALEX* and Optical Light Curves of WX LMi,  
SDSSJ103100.5+202832.2 and SDSSJ121209.31+013627.7<sup>1</sup>**

Albert P. Linnell<sup>2</sup>, Paula Szkody<sup>2</sup>, Richard M. Plotkin<sup>2</sup>, Jon Holtzman<sup>3</sup>, Mark Seibert<sup>4</sup>,  
Thomas E. Harrison<sup>3</sup>, Steve B. Howell<sup>5</sup>

**ABSTRACT**

*GALEX* near ultraviolet (NUV) and far-ultraviolet (FUV) light curves of three extremely low accretion rate polars show distinct modulations in their UV light curves. While these three systems have a range of magnetic fields from 13 to 70 MG, and of late type secondaries (including a likely brown dwarf in SDSSJ121209.31+013627.7), the accretion rates are similar, and the UV observations imply some mechanism is operating to create enhanced emission zones on the white dwarf. The UV variations match in phase to the two magnetic poles viewed in the optical in WX LMi and to the single poles evident in the optical in SDSSJ121209.31+013627.7 and SDSSJ103100.55+202832.2. Simple spot models of the UV light curves show that if hot spots are responsible for the UV variations, the temperatures are on the order of 10,000-14,000K. For the single pole systems, the size of the FUV spot must be smaller than the NUV and in all cases, the geometry is likely more complicated than a simple circular spot.

*Subject headings:* binaries: close — novae, cataclysmic variables — stars: individual (WX LMi, SDSSJ103100.55+202832.2, SDSSJ121209.31+013627.7) — ultraviolet:stars — white dwarfs

---

<sup>2</sup>Department of Astronomy, University of Washington, Box 351580, Seattle, WA 98195, szkody@astro.washington.edu, plotkin@astro.washington.edu, linnell@astro.washington.edu

<sup>3</sup>Department of Astronomy, New Mexico State University, Box 30001, MSC 4500, Las Cruces, NM 88003, tharriso@nmsu.edu, holtz@nmsu.edu

<sup>4</sup>Observatories Carnegie Institute of Washington, 813 Santa Barbara St., Pasadena CA 91101, mseibert@ociw.edu

<sup>5</sup>National Optical Astronomy Observatories, 950 N. Cherry Avenue, Tucson, AZ 85726, howell@noao.edu

<sup>1</sup>Based on observations made with the NASA Galaxy Evolution Explorer. *GALEX* is operated for NASA by the California Institute of Technology under NASA contract NAS5-98034.

## 1. Introduction

The cataclysmic variables with very low mass transfer rates ( $10^{-13}$ - $10^{-14}$   $M_{\odot}$   $\text{yr}^{-1}$ ) and highly magnetic ( $>10\text{MG}$ ) white dwarfs have been termed LARPS (Low Accretion Rate Polars; Schwöpe et al. 2002). Since the low mass transfer means the accretion luminosity is low, the individual stellar components can be viewed. Thus, these systems provide a unique comparison to widely separated binaries for the study of how angular momentum losses and heating of the white dwarf affect the binary evolutionary scenario. While normal polars can reach mass accretion rates close to those of LARPS when they undergo long periods of low mass transfer, the main difference between LARPS and normal polars in low states appears to be the temperature of the white dwarf. Ultraviolet observations of normal polars have shown temperatures of 11-14,000K for their white dwarfs (Araujo-Betancor et al. 1995). In contrast, the white dwarfs in the LARPS are less than 10,000K (Schmidt et al. 2005, 2007, hereafter S05, S07; Vogel et al. 2007, hereafter V07; Schwöpe et al. 2009, hereafter Sw09). These low temperatures imply that compressional heating has not taken place and so these objects have been suggested to be pre-Polars (S05) or PREPs (Sw09). Figure 5 of Sw09 shows a nice plot of the temperatures of 9 PREPs compared to normal polars and accreting non-magnetic white dwarfs that illustrates this difference. However, the terminology and behavior is not always so cleanly separated. The system SDSS121209.31+013627.7 (Schmidt et al. 2005b; Burleigh et al. 2006; hereafter B06) also has a low accretion rate and a low white dwarf temperature but has a brown dwarf secondary. Its evolutionary path has been suggested to be either a polar in a low state or a PREP. In addition, the recent observation of enhanced activity levels in the LARP SDSSJ204827.9+005008.9 (Honeycutt et al. 2010) suggest that it may not be a LARP/PREP or that even PREPs can have different levels of activity.

A secondary criteria for a LARP/PREP is the secondary underfilling its Roche lobe so that Roche lobe overflow does not occur (S05; S07; Sw09). This is generally determined from the system having an spectral type too late to fill the lobe if it has a normal size for its type, as well as the absence of narrow components in the emission lines that can be traced to a stream. However, the Honeycutt et al. (2010) study found evidence for a stream in SDSSJ204827.9+005008.9, although they could not determine if the system had entered an increased state of mass transfer at the time. While the low accretion rates and sizes of the secondaries imply no Roche lobe overflow, there could likely still be some accretion from the stellar wind of the secondary that is funnelled by the high field of the white dwarf (Li et al. 2004). The work of Webbink & Wickramasinghe (2005) using considerations of energy, magnetic fields, separations and lifetimes supports a wind model for the LARPS. In this study, we are not so concerned with the correct classification of our objects as LARPS, PREPs or normal polars in low states, or how the accretion might occur, but rather with

the effects of low levels of accretion on the white dwarf.

These effects are visible through time-resolved UV observations. Accretion spots with temperatures of 30,000-70,000K are easily visible on normal polars even during their sporadic low states of accretion with  $\dot{M} \sim 10^{-12} M_{\odot} \text{ yr}^{-1}$  (Araujo-Betancor et al. 2005; Gänsicke et al. 2006) as large amplitude modulations of the UV light. However, it was somewhat surprising to find that similar modulations were apparent for EF Eri (Szkody et al. 2006) which had been in a low state for seven years with  $\dot{M}$  of  $10^{-13} M_{\odot} \text{ yr}^{-1}$  and the LARP MQ Dra with an even lower  $\dot{M}$  of  $10^{-14} M_{\odot} \text{ yr}^{-1}$  (Szkody et al. 2008). While the UV light curves could be approximately matched with either hot spots or cyclotron components (Campbell et al. 2008), each interpretation has its problems: the hot spots require different sizes and geometries while the cyclotron origin requires much higher magnetic fields in the UV than are apparent in the optical. In order to further study the effects of this low level accretion, we used *GALEX* to obtain UV observations of two additional LARPS (WX LMi and SDSSJ103100.55+202832.2) and the system SDSSJ121209.31+013627.7. For convenience, we will refer to the SDSS objects as SDSS1031 and SDSS1212. The known parameters for the three systems are listed in Table 1. While all three of these objects have comparable low mass accretion rates, they present differences in magnetic field strength, white dwarf temperature, spectral type of secondary and orbital period.

## 2. Observations

The observational data include ground-based APO *B, V, R, I* light curves and FUV and NUV *GALEX* light curves. The *GALEX* observations took place on 2008 Feb 16, 23 and April 5 (Table 2 provides a summary of the times). Images in both the near ultraviolet (NUV) detector (1750-2800Å) and the far ultraviolet (FUV) detector (1350-1750Å) (Martin et al. 2005) were obtained for each source. The time-tag data were calibrated in 240s intervals (120s for the NUV of SDSSJ1212) and phased according to the spectroscopic ephemeris given in V07 for WX LMi, and to the photometric ephemeris given in B06 for SDSS1212. The phasing for SDSS1212 is accurate to  $\pm 0.14$  phase at the time of the *GALEX* observations. For SDSS1031, the ephemeris is not known with enough accuracy to phase to prior data so arbitrary phasing was used with the period of S07. The phased datapoints were then binned into 10, 15 and 20 phase bins to optimize the S/N vs time resolution. The magnitudes for each binning were then measured using a 9 pixel radius aperture with the IRAF<sup>2</sup>

---

<sup>2</sup>IRAF (Image Reduction and Analysis Facility) is distributed by the National Optical Astronomy Observatories, which are operated by AURA, Inc., under cooperative agreement with the National Science

routine *qphot*, using an average sky over the entire phase interval. Flux conversions for the modeling were done using the values given in the *GALEX* online documentation<sup>3</sup> (FUV  $m_0=18.82=1.40\times 10^{-15}$  ergs  $\text{cm}^{-2} \text{s}^{-1} \text{\AA}^{-1}$  and NUV  $m_0=20.08=2.06\times 10^{-16}$  ergs  $\text{cm}^{-2} \text{s}^{-1} \text{\AA}^{-1}$ ).

Optical photometry in 2008 April and May (Table 2) was obtained for WX LMi and SDSSJ1031 using the NMSU 1m telescope at Apache Point Observatory. Differential light curves in *BVRI* filters were made from nearby comparison stars on the same CCD frames. For WX LMi, one of the comparison stars used was the calibrated star A from Schwarz et al. (2001) so that the differential magnitudes could be transformed to actual *BVRI* values.

### 3. The Analysis Program

As in our previous spot models of EF Eri and MQ Dra, the BINSYN program suite (Linnell & Hubeny 1996) was used to calculate synthetic light curves that could fit the observations. Recent papers (Linnell et al. 2007; 2008) illustrate details of its application to cataclysmic variables, and Hoard et al. (2005) describe its use in simulating hot spots on the magnetic white dwarf YY Dra. While a hot spot may be multi-temperature and have a complicated shape as well as radiation influenced by the strong magnetic field, we attempted to minimize the free parameters by using a first approximation to the spot parameters with a circular, isothermal hot spot (with a white dwarf spectral energy distribution). As our intent is to determine if a hot spot alone can account for the FUV and NUV light curves, we ignore cyclotron effects. The harmonics will affect the optical light curves to various degrees (depending on where they appear in the various filters) and can add to or dominate the observed amplitude of variation from the spot.

In general, if the objective of the analysis is only to fit the light variations (the absolute fluxes are unknown), the light curves are normalized to a light maxima of 1.0, and then BINSYN can be used to calculate monochromatic light curves. In this mode, the program represents the stellar components as a sum of black body contributions from local photospheric values of  $T_{\text{eff}}$  determined by adopted values of bolometric albedos and gravity darkening exponents. No synthetic spectra are needed.

However, the WX LMi light curves required special considerations, since those light curves are absolute flux measurements. Their simulation, via synthetic photometry from

---

Foundation.

<sup>3</sup>See <http://galexgi.gsfc.nasa.gov/tools/index.html>

synthetic spectra, produced calculated absolute flux values outside the Earth’s atmosphere, using transmission profiles of the filters and the quantum efficiency of the CCD, and the distance of the system. In previous papers the synthetic spectra input to BINSYN were calculated using TLUSTY (Hubeny 1988) and SYNSPEC (Hubeny et al. 1994). However, the Hubeny TLUSTY WD models do not extend to cooler than 8000K. Fortunately, cool WD models have been calculated by Bergeron et al. (1991; 1995). Dr. Bergeron kindly provided a set of 40 WD synthetic spectra with  $\log g=8.0$  and  $T_{\text{eff}}$  ranging from 17,000K to 1500K. Each synthetic spectrum includes Eddington flux values ( $\text{erg sec}^{-1} \text{cm}^{-2} \text{hz}^{-1}$ ) at 1788 unequally-spaced wavelengths between  $43\text{\AA}$  and  $95,000\text{\AA}$ . Synthetic spectra similar to these have been used in the synthetic WD photometry of Holberg & Bergeron (2006). We produced corresponding synthetic spectra in wavelength units ( $\text{erg sec}^{-1} \text{cm}^{-2} \text{\AA}^{-1}$ ).

We input WD synthetic spectra with  $T_{\text{eff}}$  values of 6000K, 6500K, 7000K, 7500K, and 8000K to BINSYN; the program then used an adopted WD  $T_{\text{eff}}$ , within the above range, and interpolated among the input spectra to produce a synthetic WD spectrum of the assigned  $T_{\text{eff}}$ . As representation of the hot spots on the WD (the impact regions of the incoming mass from the secondary) requires additional synthetic WD spectra, we added input WD synthetic spectra with  $T_{\text{eff}}$  values of 10,000K, 11,000K, and 12,000K.

Synthetic spectra to represent the secondary star present a separate problem. If the secondary fills its Roche lobe,  $T_{\text{eff}}$  and  $\log g$  vary over the photosphere as determined by the values of gravity darkening and bolometric albedo (temperature variation due to irradiation by the WD is negligible). As BINSYN needs synthetic spectra for cool photospheres over a range of  $T_{\text{eff}}$  and  $\log g$ , we downloaded a database of MARCS <sup>4</sup> synthetic spectra for this purpose. Each MARCS synthetic spectrum tabulates physical flux values ( $\text{erg sec}^{-1} \text{cm}^{-2} \text{\AA}^{-1}$ ) for 101,125 wavelengths unequally spaced between  $900\text{\AA}$  and  $200,007\text{\AA}$  and we then prepared corresponding spectra in Eddington flux units. To permit accurate interpolation to the local photospheric values of  $T_{\text{eff}}$  and  $\log g$  on the secondary star we provided BINSYN with 24 MARCS spectra for  $T_{\text{eff}}$  values of 2500K, 2700K, 2900K, 3100K, 3300K, and 3400K, and for each of these,  $\log g$  values of 3.0, 4.0, 4.5, and 5.0. The single secondary component point nearest the L1 point has an associated photospheric segment whose flux contribution is negligible. We include an input black body spectrum of 1500K which, together with the other input spectra for the secondary star, brackets this point. MARCS spectra span all other grid segments covering the secondary star. The BINSYN output includes a synthetic spectrum for the system, the WD, and the secondary star, all for an adopted orbital longitude and orbital inclination,  $i$ .

---

<sup>4</sup><http://marcs.astro.uu.se>

## 4. WX LMi

WX LMi was found in the Hamburg Quasar Survey by Reimers et al. (1999) who determined the orbital period, the spectral type of the secondary and the distance. From the spectrum and photometry, they concluded there were two accretion spots, with magnetic fields of 60 and 68 MG and the accretion rate was about 100 times less than normal polars. Further long term photometry was obtained by Schwarz et al. (2001) and modeled to determine the colatitudes ( $90\text{-}130^\circ$ ) and azimuths ( $-70$  to  $-80$ , and  $+90^\circ$ ) of the spots. These locations placed the spots slightly below the equator of the white dwarf and further from the line-of-centers between the stars than in normal high accretion rate polars. V07 used *XMM-Newton* to obtain X-ray data as well as some near UV photometry using the optical monitor (OM) UV filters at 2910 and 3440Å. They also used optical spectra to establish an upper limit to the temperature for the white dwarf of 8000K and to constrain the cyclotron model and accretion rate. They concluded that the low accretion rate was consistent with accretion resulting from wind loss from the secondary. Their model found small (40 km radius) accretion spots at similar locations to that of Schwarz et al. (2001) but the X-ray vs UV modulations and the hardness ratios were not consistent with heated spots. The X-ray emission was assumed to originate from both coronal activity on the secondary and from the accretion regions.

The *GALEX* data explore the regime between the X-ray and OM filters. The UV light curves (with 15 phase bins) are shown in Figure 1 along with the optical data obtained about 2 months later. The double-humped light curve variation that has been taken to be evidence of the accretion areas undergoes an interesting variation with wavelength. Figure 1 shows the progression from a double-humped curve in the I filter to a very low level of variability in the optical *B* and then an increasing variation as the FUV is reached. The phasing here is spectroscopic (phase 0 is inferior conjunction of the secondary) so the primary pole is evident between phase 0.8 and 0.9, the secondary pole near phase 0.3 and both poles are self-eclipsed near phase 0.6. The FUV shows slightly higher flux for the secondary pole than the primary, which corroborates what V07 regarded as a puzzle i.e. that the secondary spot seems hotter than the primary one. The dips at phase 0.3 in *V* and *B* are related to the cyclotron features at 5950Å and 5220Å which appear in these filters and change strength during the orbit due to the changing viewing angle.

### 4.1. Model Parameters

V07 determined or adopted some of the parameters needed for a simulation of the WX LMi system including the orbital period,  $P$ ;  $M_{\text{wd}} = 0.6M_\odot$  (adopted);  $M_s = 0.179M_\odot$ ;

$T_{\text{eff,wd}} = 8000\text{K}$ ; and  $T_{\text{eff,s}} = 3300\text{K}$ , appropriate to an M4.5 spectral type. They also determined some of the spot parameters associated with the magnetic field, including  $\beta(1, 2) = 145, 135$ , the spot colatitudes, and  $\psi(1, 2) = 60, -95$ , the spot azimuths. These parameters are listed in Table 3. The mass transfer rate ( $\dot{M}$ ) in WX LMi ( $\sim 1.5 \times 10^{-13} M_{\odot} \text{ yr}^{-1}$ ; V07), is listed as a system parameter in Table 3 but is not needed in the analysis.

$M_s = 0.179 M_{\odot}$ , listed in V07 (Table 2) for a secondary star of spectral type M4.5, differs slightly from the calibration of Knigge (2006; 2007),  $M_s = 0.200 M_{\odot}$  at the WX LMi orbital period, but we preserve the value  $0.179 M_{\odot}$  for consistency with the other V07 parameters. We have assigned error bars in Table 3 from the range of  $M_s$  values in Table 2 of V07. We adopt a secondary component model which fills its Roche lobe ( $\Omega(s)$ , Table 3). V07 describe WX LMi as a pre-polar candidate, appropriate to the very small  $\dot{M}$ , and underfilling its Roche lobe. It is convenient for our analysis to assume a secondary star which fills its Roche lobe; after obtaining a solution we tested the sensitivity of our assumption by performing a simulation in which the secondary underfills its Roche lobe.

The adopted value of  $M_{\text{wd}} = 0.6 M_{\odot}$  has no assigned error bars. The radius of a zero temperature homogeneous Hamada-Salpeter carbon  $0.6 M_{\odot}$  WD is  $0.0120 R_{\odot}$  (Panei et al. 2000); we adopt this value with no change for the very small correction to a 8000K WD. The WD Roche potential,  $\Omega_{\text{wd}}$ , Table 3, produces the required  $R_{\text{wd}}$ . The Table 3  $T_{\text{eff,wd}} = 8000\text{K}$  was determined by V07 but they state that the true value is less than 8000K; they were unable to pursue this topic because of their lack of lower temperature models. V07 show that  $i$  is less than  $72^\circ$ ; the presence of detectable ellipticity in the light curve suggests a fairly large  $i$ ; we adopt  $i = 70^\circ$ . Figure 2 shows the final system synthetic spectrum at orbital phase 0.0. This synthetic spectrum can be compared with the observed spectrum (Figure 1 of V07).

#### 4.2. $B, V, R, I$ Synthetic Photometry light curves

We calculated and stored system synthetic spectra for 33 orbital longitudes for each test simulation. Each synthetic spectrum extended from  $800\text{\AA}$  to  $10,000\text{\AA}$  and included Eddington flux values at  $1\text{\AA}$  spacing, produced by interpolation within the input spectra to BINSYN and integrated, within BINSYN, over the photospheric segments visible to the observer, and with an adopted limb darkening of 0.6. Our initial simulation neglected any hot spots on the WD as we expected possible hot spots only to make a negligible contribution to the  $B, V, R, I$  light curves. We subsequently verified this expectation.

The APO filter transmission curves and the quantum efficiency curve of the CCD used

for the ground-based photometry were digitized by hand. The CCD quantum efficiency drops to 0.0 at 10,000Å and this sets the upper wavelength limit for the simulation. We also produced comparable transmission curves for the FUV and NUV filters using the *GALEX* calibrations<sup>5</sup>.

Program SYNPHOT, within the BINSYN package, produces the integrated physical flux for each filter resulting from a system synthetic spectrum incident on the APO filter set and CCD, given by the expression

$$F_s = \frac{\int S(\lambda)f(\lambda)d\lambda}{\int S(\lambda)d\lambda}$$

where  $S(\lambda)$  is the photometric system response function and  $f(\lambda)$  is the synthetic spectrum incident flux.

Numerical integration requires a value for the filter transmission and CCD response at each tabular wavelength of the system synthetic spectrum. We used the Numerical Recipes (Press et al. 1986) program **Spline** to fit each digitized filter transmission curve as well as the CCD response curve, and the Numerical Recipes routine **Splint** to produce the required transmission or response at the synthetic spectrum wavelengths.

The quantity to compare with an observed light curve is the integrated flux divided by  $D^2$ , where  $D$  is the distance to the system in cgs units. We initially adopted the V07 determination of 100 pc. The initial test showed rough agreement between simulation and observed light curves with variable cyclotron contributions. The calculated light curves were systematically too bright in  $B$ ,  $R$ , and  $I$ , with a strong cyclotron contribution in  $V$ . We varied the assumed distance to obtain an optimum overall fit by eye and determined a revised distance of 107 pc. This value is in very close agreement with the V07 value of 104 pc in their Table 2 for the M4.5 spectral type adopted for the secondary star in this study.

The final light curves, compared with the observations, are shown in Figure 3 (note the change in ordinate scale in Figure 3d). Cyclotron emission dominates the  $V$  band light curve. This is in agreement with the V07 cyclotron model, their Figure 7. The same Figure 7 indicates some cyclotron contribution to the  $B$ ,  $R$ , and  $I$  light curves.

Figure 3d shows that the synthetic light curve has slightly too much flux for the adopted distance of 107 pc. As Figure 2 shows, the secondary component spectrum rises rapidly to a peak near 10,000Å. A small departure of the actual WX LMi secondary component from the adopted model could explain this residual.

---

<sup>5</sup><http://galexgi.gsfc.nasa.gov/docs/instrument.html>



The inclination cannot be increased more than a few degrees without producing eclipses; a reduction in the inclination decreases the light curve amplitude and increases the absolute flux level. We regard the adopted  $i = 70^\circ$  as optimum, considering the light curve contributions by cyclotron emission.

### 4.3. NUV and FUV Synthetic Photometry light curves

Figure 7 of V07 makes no prediction concerning cyclotron emission in the FUV or NUV, and the contribution of the secondary component becomes negligible shortward of about  $3500\text{\AA}$  so it does not contribute in the NUV or FUV.

We adopted circular models for the two hot spots and experimented with their  $T_{\text{eff}}$  values and angular radii. Initial simulations suggested a WD  $T_{\text{eff}} = 7800\text{K}$ . Initial choice of spot  $T_{\text{eff}}$  values of  $12,000\text{K}$  produced a FUV light curve amplitude that was much too large. Lower temperature spots require larger radii to preserve the light curve amplitude, particularly in the NUV. Eventually we found an acceptable fit with spot radii of  $32^\circ$  and  $T_{\text{eff}}$  values of  $10,000\text{K}$ . A final correction of the WD  $T_{\text{eff}}$  to  $7900\text{K}$  produced the best fit, by eye (Figure 2 has a WD with  $T_{\text{eff}}$  of  $7900\text{K}$ ). The FUV and NUV light curves are shown in Figure 4 and the final spot parameters are in Table 4.

The spots are large; a view of the WD at orbital phase 0.0 is in Figure 5. We suggest that this result is not inconsistent with the small  $\dot{M}$  and impacting stream from the secondary component wind rather than a stream emerging through the L1 point. While our spot sizes are much larger than those of V07, (their estimate of the accretion area was about 40 km in radius, whereas our  $32^\circ$  spots are about 4700 km in radius), their estimate was based on the X-ray and beamed cyclotron regions. These areas are typically much smaller spots than the heated areas visible in the UV (Gänsicke et al. 2006). Time-resolved UV spectropolarimetry will be required to obtain further knowledge of cyclotron effects in the UV. For the field strength of 68 MG, the  $n=6-8$  harmonics will be in the NUV band. This could account for some of the deviations of the fit in this band.

As a check, we recalculated the  $B, V, R,$  and  $I$  light curves with and without the spots included in the model. There was a barely detectable spot contribution to those light curves, far too small to require a revision of the model. Our model does not prove that hot spots are the cause of the NUV and FUV light variation, it only demonstrates that our adopted parameters can approximate the observed light variations. The deviations likely indicate that the spots have more complicated geometries than our simple assumption of a circular shape.

#### 4.4. Does the secondary component fill its Roche lobe?

Our model assumes the secondary component fills its Roche lobe. As a test we changed the value of  $\Omega_s$  (Table 3), so that the volume of the secondary was 95% of the initial model value which filled the Roche lobe. Recalculation of the  $B, V, R, I$  light curves showed that the amplitudes are almost unaffected. A slight amplitude reduction of the  $I$  light curve is barely detectable. Further reducing the volume to 90% produces the changes shown in Figure 6. Thus, the secondary can underfill the Roche lobe by a small amount without reducing the theoretical light curve amplitudes sufficiently to be in disagreement with the observed light curve. However, if it underfills by a large factor, the light curve amplitude, especially in  $I$ , would be too small due to the reduced ellipticity of the secondary. If there is some contribution of the  $n=2$  harmonics in the  $I$  filter, the cyclotron would dilute the ellipsoidal variation from the secondary, which would necessitate an even larger filling factor, although the variation from the cyclotron would then add to the variability as well.

### 5. SDSS1031

As with the majority of the LARPS, SDSS1031 was discovered by searches through the SDSS spectroscopic survey (S07). The variations in the polarimetry and photometry determined a short orbital period and the spacing of the cyclotron harmonics revealed the magnetic field. The spectral fluxes between the cyclotron harmonics placed limits on the white dwarf temperature and the late spectral type of the secondary (Table 1 summarizes these values). Its very short period makes it unusual among the LARPS (Figure 5 of Sw09), and may present problems for its evolution as a PREP. However, its low accretion rate, cool white dwarf and late type secondary which underfills its Roche lobe (S07) all match the primary characteristics of LARPS. SDSS1031 shares many characteristics of the short period normal polar EF Eri which has mostly been in a low state since 1997 but does have occasional high states (Howell et al. 2006).

The UV through optical light curves of SDSS1031 are shown in Figure 7, where the arbitrary phase in UV and optical is set so that maximum light occurs roughly at phase 0. While SDSS1031 is the faintest of our three sources in the optical, the FUV magnitudes are comparable to WX LMi. The  $R$  filter shows the cyclotron variation found by S07 with some evidence of a double-humped shape indicative of beaming in an optically thin high cyclotron harmonic. The  $V$  filter shows the least orbital variation while  $B$  has an increased amplitude. The amplitude of the UV orbital modulation is much lower than in WX LMi and more asymmetrical in shape, showing a gradual rise to maximum followed by a steeper decline. If the variation is due to a hot spot, the similar amplitudes in FUV and NUV mean

that the spots must be different sizes and simple circular isothermal spots will not provide a good fit to the observations. To get a crude idea of what kind of spot would be needed, the BINSYN model was computed for the parameters shown in Table 4 and fit to the *GALEX* data binned by 10 in phase (Figure 8). The best fit obtained was with a 13,000K spot at  $-65^\circ$  latitude. The spot radius was  $10^\circ$  for the FUV and  $23^\circ$  for NUV. However, as expected, the shape of the variation is not fit well.

### 5.1. SDSS1212

Like SDSS1031, this object was found in searching through the SDSS spectra (Schmidt et al. 2005b) because the Balmer lines showed Zeeman splitting from a magnetic white dwarf as well as weak  $H\alpha$  emission. Spectroscopy by these authors revealed a period near 90 min but no secondary star was detected and an IR measurement at  $J$  implied a brown dwarf object of spectral type L5 or later. Further IR observations by Debes et al. (2006) refined the orbital period and showed a variation in the  $K$  band that could be explained with cyclotron emission from a small spot on the white dwarf. Farihi, Burleigh & Hoard (2008) modeled further IR data with an L8-T1 substellar dwarf and a white dwarf with a 7 MG field. B06 obtained X-ray observations with *Swift* which detected the source but with too low of a count rate to ascertain variability. The flux was best fit with a thermal plasma with  $kT=1.9$  keV and a luminosity of  $10^{29}$  erg  $s^{-1}$ . While this luminosity is comparable to that detected in the LARP MQ Dra (Szkody et al. 2004), and the low state of the polar AR UMA (Szkody et al. 1999), it is far larger than the X-ray luminosities of L dwarfs (Stelzer et al. 2006). The  $u, g, i$  photometry of B06 shows a single hump that increases in amplitude in the blue, with some slight indication of a second small peak half a phase later that was pointed out by Koen & Maxted (2006). The origin of the second peak is not clear; Koen & Maxted (2006) suggested a reflection effect from the secondary (since the feature seemed to increase at longer wavelengths), while B06 mention a possible second pole (but this is not evident in the IR photometry of Debes et al. (2006).

B06 model the primary optical hump as a 14,000K hot spot on the white dwarf. However, as they point out, it is not clear what provides the accretion necessary to produce the X-rays and a hot spot. A brown dwarf that underfills its Roche lobe should not produce an accretion stream nor a wind outflow. Recent photometry by Howell et al. (2008) showed that the strength of  $H\alpha$  is variable, indicating that the secondary has some activity. It may be that the secondary stars in close binaries have higher activity levels than their single counterparts due to their faster rotations in a binary system.

Our *GALEX* data on SDSS1212 (Figure 9) shows a similar single-peaked modulation

with increased amplitude in FUV over the NUV and a possible hint of a second small peak near phase 0.5. The NUV magnitude is the brightest of the three objects. Trial models with BINSYN using the B06 parameters for the  $i$ , masses, and temperature of the white dwarf revealed that the width of the hump is a clear function of the spot latitude, with greater width when the spot is in the same hemisphere as the visible pole. A good fit (Figure 10 bottom) to the NUV light curve was obtained with a 14,000K spot (the same temperature found by B06 from the optical light curves) with a radius of  $9^\circ$ , but this spot produced a FUV amplitude that was too large. Thus, as in MQ Dra (Szkody et al. 2008), a single spot size and temperature cannot fit both the NUV and FUV. If the spot temperature is kept at 14,000K, a smaller spot of  $7^\circ$  fits the FUV reasonably well (Figure 10 top). The observed light curve shows some scatter and there is a hint that the light curve is asymmetric with a slower rise than decline. The spot sizes are 1% of the white dwarf surface in FUV and 1.7% in NUV, as compared to the 5% found by B06 from their optical modeling. These numbers follow the trend of decreasing spot sizes with smaller wavelengths.

Increased time-resolution and S/N will be needed to further understand the reality and nature of the possible peak near phase 0.5. It is intriguing that this feature is evident from UV through the  $R$  band. These phases need to be targeted to determine if there is accretion related to a second pole.

## 6. Conclusions

Our UV observations of three polars with extremely low accretion rates enforce the results found from observations of EF Eri and MQ Dra i.e. that all the white dwarfs have areas of enhanced emission even with these low rates, indicating some accretion is still occurring. Despite a large range in magnetic field (7-70MG), the field is apparently strong enough in all three systems to funnel the accreting material to the magnetic pole(s) of the white dwarf. This appears to happen even in the case of SDSS1212, which likely has a brown dwarf secondary. Thus, if the accretion is via a stellar wind from the secondary that is trapped by the field of the white dwarf, it is difficult to provide a wind of this type for SDSS1212. Time-resolved spectra that would enable Doppler tomography might provide a resolution of this issue. During high states of accretion, the stream flow is usually visible as a narrow component in the Balmer emission lines which is mapped to the stream. In normal polars during their low states, high velocity components in the lines have been interpreted as structures similar to prominences close to the secondary star (Kafka et al. 2007, 2008). However, the Balmer emission in LARPS is weak to non-existent due to the low the accretion rates low so it would be difficult to construct the map.

If the increased emission evident at some phases is due to hotter temperature, simple spots of 10,000-14,000K covering a few percent of the white dwarf surface can approximate the UV light curves, although the geometries of the spots require a more complex model shape than simply circular. Alternatively, if there is a large range in field strengths in the white dwarfs, there could be contributions to the UV from higher cyclotron harmonics. Improved UV cyclotron models will be needed to test this possibility. Since these objects are too faint for *GALEX* spectra or high S/N time-resolved UV light curves that would merit detailed models of the shape or of pursuing cyclotron radiation, further work will require UV spectra and polarimetry with larger telescopes.

Support for this research was provided by NASA *GALEX* grant NNX08AM07G. We gratefully acknowledge Pierre Bergeron for providing cool white dwarf models, the MARCS database for access to their spectra, Eric Bullock for work with some of the data files, and Mark Klaene for providing optical filter curves.

## REFERENCES

- Araujo-Betancor, S. et al. 2005, *ApJ*, 622, 589
- Bergeron, P., Wesemael, F. & Fontaine, G. 1991, *ApJ*, 367, 253
- Bergeron, P., Saumon, D. & Wesemael, F. 1995, *ApJ*, 443, 764
- Burleigh, M. R. et al. 2006, *MNRAS*, 373, 1416 (B06)
- Campbell, R. K., Harrison, T. E., Schwope, A. D. & Howell, S. B. *ApJ*, 672, 531
- Debes, J. H., Lopez-Morales, M., Bonanos, A. Z. & Weinberger, A. J. 2006, *ApJ*, 647, L147
- Farihi, J., Burleigh, M. R. & Hoard, D. W. 2008, *ApJ*, 674, 421
- Gänsicke, B. T., Long, K. S., Barstow, M. A. & Hubeny, I. 2006, *ApJ*, 639, 1039
- Hoard, D. W., Linnell, A. P., Szkody, P. & Sion, E. M. 2005, *ApJ*, 130, 214
- Holberg, J. B. & Bergeron, P. 2006, *AJ*, 132, 1221
- Honeycutt, R. K., Kafka, S. & Tappert, C. 2010, *BAAS*, 215, 416.19
- Howell, S. B., Walter, F. M., Harrison, T. E., Huber, M. E., Becker, R. H. & White, R. L. 2006, *ApJ*, 652, 709
- Howell, S. B., Harrison, T. E., Huber, M. E., Szkody, P., Walter, F. M. & Harbeck, D. 2008, *AJ*, 136, 2541
- Hubeny, I. 1988, *Comp. Phys. Comm.*, 52, 103

- Hubeny, I., Lanz, T., & Jeffery, C. S. 1994, in Newsletter on Analysis of Astronomical Spectra No. 20, ed. C. S. Jeffery (CCP7;St. Andrews: St . Andrews Univ.), 30
- Kafka, S., Howell, S. B., Honeycutt, R. K. & Robertson, J. W. 2007, AJ, 133, 1645
- Kafka, S. Ribeiro, T., Baptista, R., Honeycutt, R. K. & Robertson, J. W. 2008, ApJ, 688, 1302
- Koen, C. & Maxted, P. F. L. 2006, MNRAS, 371, 1675
- Knigge, C. 2006, MNRAS, 373, 484
- Knigge, C. 2007, MNRAS, 382, 1982
- Li, J., Wu, K. W. & Wickramasinghe, D. T. 1994, MNRAS, 268, 61
- Linnell, A. P. & Hubeny, I. 1996, ApJ, 471, 958
- Linnell, A. P., Godon, P., Hubeny, I., Sion, E. M. & Szkody, P. 2007, ApJ, 662, 1204
- Linnell, A. P., Godon, P., Hubeny, I., Sion, E. M., Szkody, P. & Barrett, P. E. 2008, ApJ, 676, 1226
- Martin, D. C. et al. 2005, ApJ, 619, L1
- Panei, J. A., Althaus, L. G. & Benvenuto, O. G. 2000, A&A, 353, 970
- Press, W. H., Flannery, B. P., Teukolsky, S. A. & Vetterling, W. T. 1986, (Cambridge; University Press, Cambridge)
- Reimers, D., Hagen, H.-J. & Hopp, U. 1999, A&A, 343, 157
- Schmidt, G. D. et al. 2005, ApJ, 630, 1037 (S05)
- Schmidt, G. D. et al. 2005b, ApJ, 630, L173
- Schmidt, G. D. et al. 2007, ApJ, 654, 521 (S07)
- Schwarz, R., Schwobe, A. D. & Staude, A. 2001, A&A, 374, 189
- Schwobe, A. D. et al, 2002, in ASP Conf. Vol 261, The Physics of Cataclysmic Variables and Related Objects, ed. B. T. Gänsicke, K. Beuermann, & K. Reinsch (San Francisco:ASP), 102
- Schwobe, A. D., Gomez-Moran, A. N., Schreiver, M. R. & Gänsicke, B. T. 2009, A&A, 500, 867 (Sw09)
- Stelzer, B., Micela, G., Flaccomio, E. R. N. & Jayawardhana, R. 2006, A&A, 448, 293
- Szkody, P. et al. 1999, ApJ, 520, 841
- Szkody, P. et al. 2004, AJ, 128, 2443
- Szkody, P. et al. 2006, ApJ, 646, L147

Szkody, P. et al. 2008, *ApJ*, 683, 967

Vogel, J., Schwope, A. D. & Gänsicke, B. T. 2007, *A&A*, 464, 647 (V07)

Webbink, R. F. & Wickramasinghe, D. T. 2005, in *ASP Conf. Ser. 330, The Astrophysics of Cataclysmic Variables and Related Objects*, ed. J. M. Hameury & J. P. Lasota (San Francisco:ASP), 137

Table 1. Objects

Parameter	WX LMi	SDSS1031	SDSS1212
$P_{orb}$ (hr)	2.78	1.37	1.47
Optical Mag	$V=16.97$	$g=18.26$	$g=17.99$
$T_{wd}$ (K)	$<8000$	9000	9500
B (MG)	61,70	42	7
Sec Type	dM4.5	$\geq$ dM6	L8-T1
d (pc)	100	270-380	120
$\dot{M}$ ( $\times 10^{-13} M_{\odot} \text{ yr}^{-1}$ )	1.5	1.5-3	1
Ref <sup>a</sup>	1, 2	3	4, 5, 6

<sup>a</sup>(1) Reimers et al. (1999), (2) Vogel et al. (2007), (3) Schmidt et al. (2007), (4) Schmidt et al. (2005b), (5) Burleigh et al. (2006), (6) Farihi et al. (2008)



Table 2. Summary of 2008 Observations

Object	Date	UT	Data
WX LMi	Feb 16	10:23-20:42	<i>GALEX</i> NUV, FUV 7 visits
WX LMi	Apr 29	03:57-08:56	<i>BVRI</i> 39 exposures
SDSS1031	Feb 23	10:01-20:19	<i>GALEX</i> NUV, FUV 7 visits
SDSS1031	May 5	05:04-08:15	<i>BVR</i> 12 exposures
SDSS1212	Apr 5	11:14-23:01	<i>GALEX</i> NUV, FUV 8 visits

Table 3. WX LMi Model System Parameters

parameter	value	parameter	value
$M_{\text{wd}}$	$0.60M_{\odot}$	$T_{\text{eff},s}(\text{pole})$	$3300\pm 100\text{K}$
$M_s$	$0.179\pm 0.4M_{\odot}$	$T_{\text{eff},s}(\text{point})$	$1640\text{K}$
$\dot{M}$	$1.5\times 10^{-13}M_{\odot}\text{yr}^{-1}$	$T_{\text{eff},s}(\text{side})$	$3259\text{K}$
P	$0.11592364$ days	$T_{\text{eff},s}(\text{back})$	$3133\text{K}$
$D$	$0.920131R_{\odot}$	$r_s(\text{pole})$	$0.234R_{\odot}$
$\Omega_{\text{wd}}$	76.65	$r_s(\text{point})$	$0.348R_{\odot}$
$\Omega_s$	2.4625438	$r_s(\text{side})$	$0.250R_{\odot}$
$i$	$70^{\circ}$	$r_s(\text{back})$	$0.280R_{\odot}$
$T_{\text{eff,wd}}$	$7900\pm 100\text{K}$	$\log g_s(\text{pole})$	4.95
$r_{\text{wd}}$	$0.0120R_{\odot}$	$\log g_s(\text{point})$	1.16
$\log g_{\text{wd}}$	8.05	$\log g_s(\text{side})$	4.89
$A_{\text{wd}}$	1.0	$\log g_s(\text{back})$	4.67
$A_s$	0.6	$\beta(1,2)$	$145, 135^{\circ}$
$\beta_{\text{wd}}$	0.25	$\psi(1,2)$	$60, -95^{\circ}$
$\beta_s$	0.08		

Note. — wd refers to the WD;  $s$  refers to the secondary star.  $D$  is the component separation of centers,  $\Omega$  is a Roche potential.  $A$  values are bolometric albedos,  $\beta_{\text{wd}}$  and  $\beta_s$  values are gravity-darkening exponents,  $\beta(1,2)$  and  $\psi(1,2)$  are spot colatitudes and spot azimuths. See the text for a discussion.

Table 4. Model Parameters

Parameter	WX LMi	SDSS1031	SDSS1212
WD $T_{eff}$	7900K	9500K	9500
WD mass ( $M_{\odot}$ )	0.6	0.6	0.6
WD radius ( $R_{\odot}$ )	0.012	0.012	0.012
WD log g	8.0	8.0	8.0
Sec mass ( $M_{\odot}$ )	0.18	0.08	0.08
i ( $^{\circ}$ )	70	70	70
Spot $T_{eff}$	10,000; 10,000K	13,000K	14,000K
Spot latitude	-55; -45 $^{\circ}$	-65 $^{\circ}$	-15 $^{\circ}$
Spot ang rad FUV	32 $^{\circ}$ ; 32 $^{\circ}$	10 $^{\circ}$	7 $^{\circ}$
Spot ang rad NUV	32 $^{\circ}$ ; 32 $^{\circ}$	23 $^{\circ}$	9 $^{\circ}$

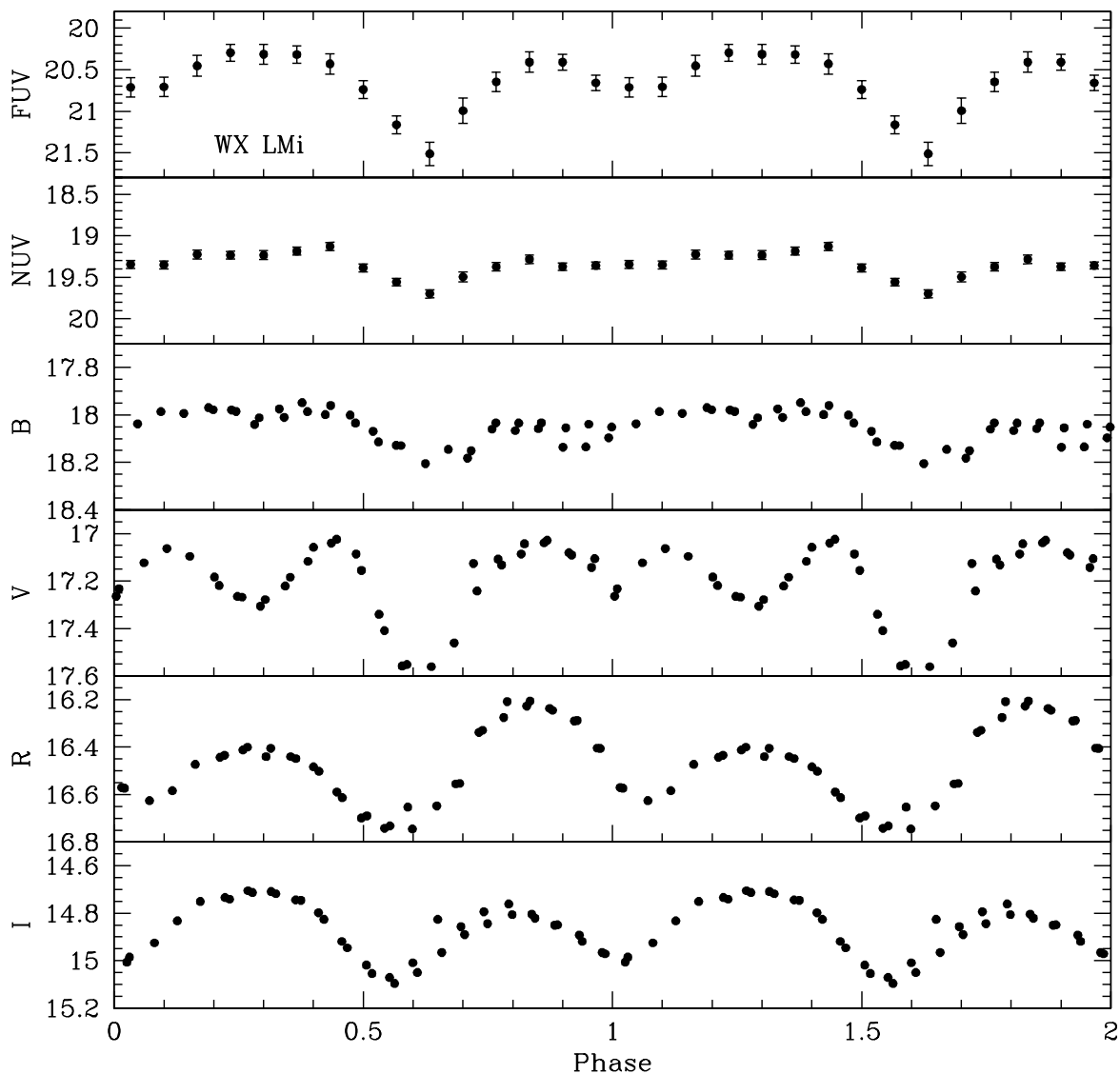


Fig. 1.— *GALEX* FUV and NUV and optical *B*, *V*, *R*, *I* filter light curves as a function of phase (phase 0 is inferior conjunction of secondary from V07) for WX LMi. Light curves are repeated from phases 1.0 to 2.0. Error bars for the optical data are smaller than the points. The comparison star for *B*, *V*, *R*, *I* is star A from Schwarz et al. 2001.

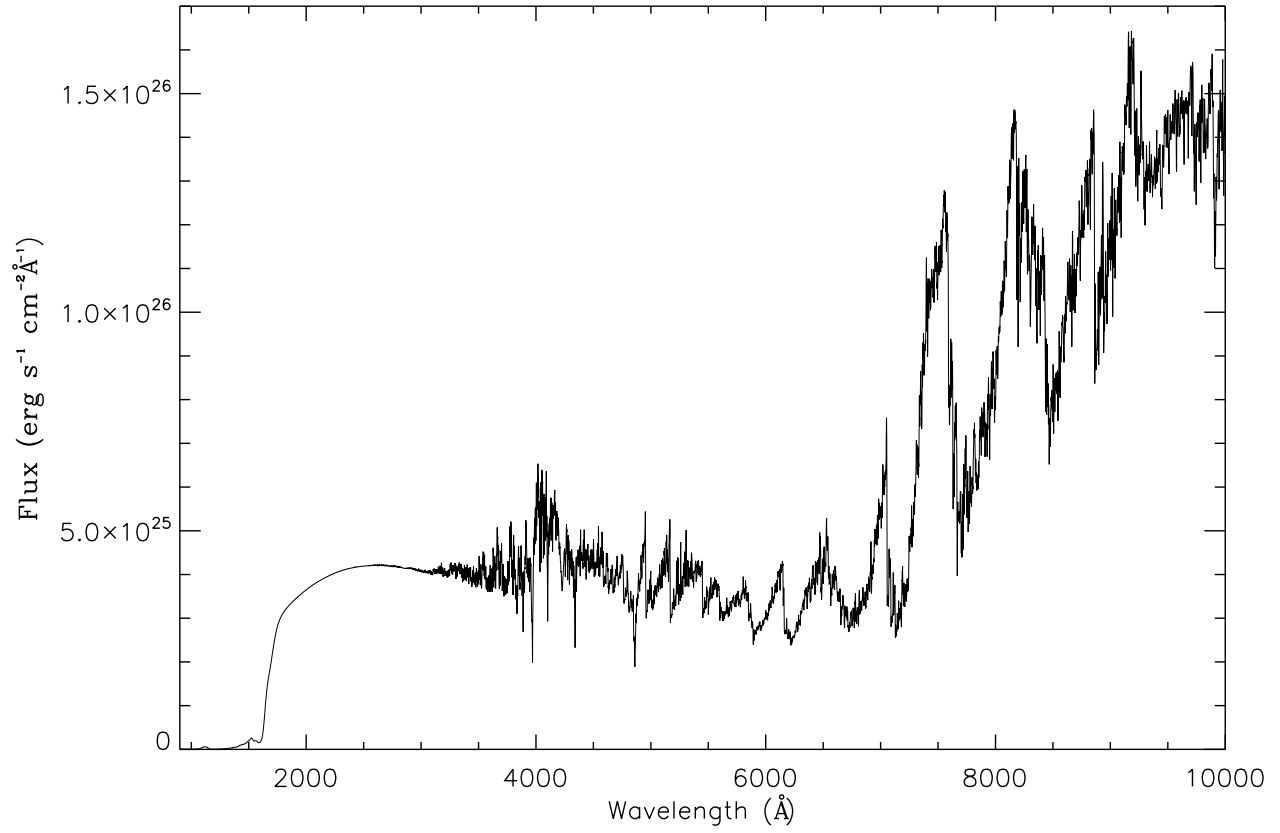


Fig. 2.— Synthetic spectrum of WX LMi at orbital phase 0.0. The flux is as seen at the star.

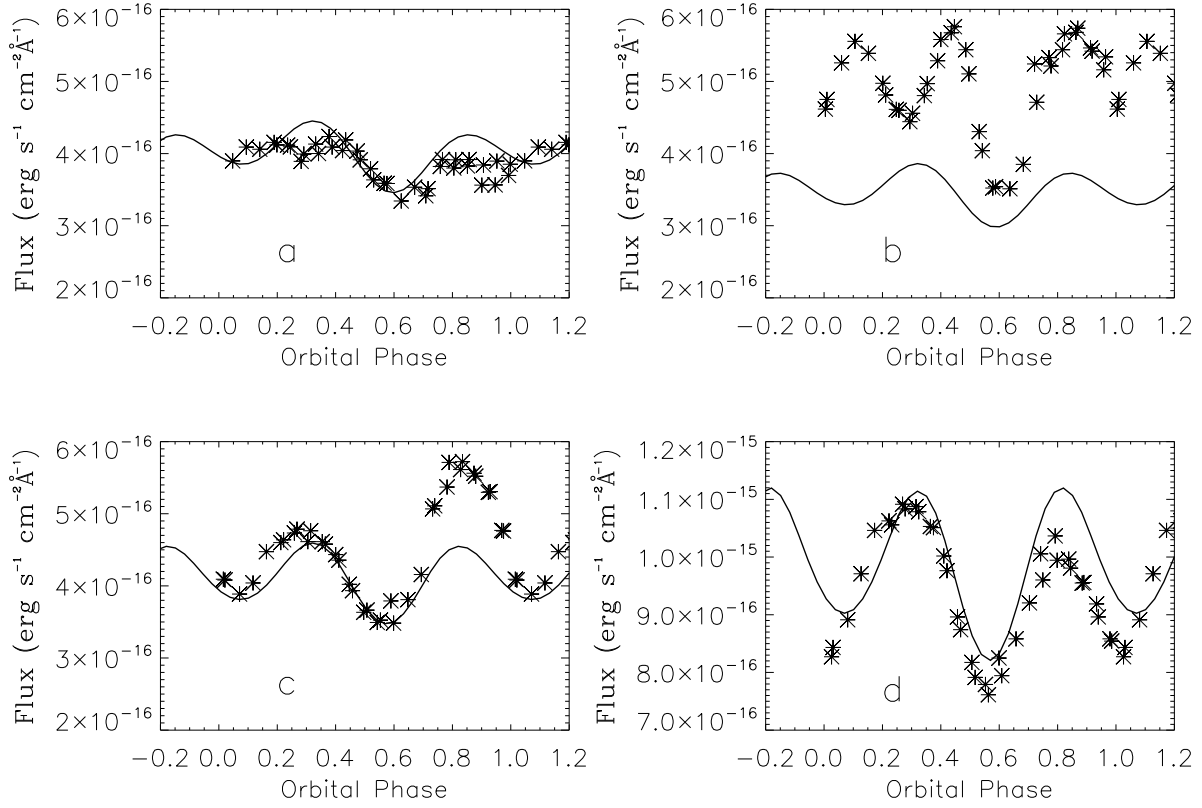


Fig. 3.— Synthetic photometry light curves of WX LMi as seen from 107 pc; *B* filter (a); *V* filter (b); *R* filter (c) and *I* filter (d). Note the change in ordinate scale for the *I* light curve.

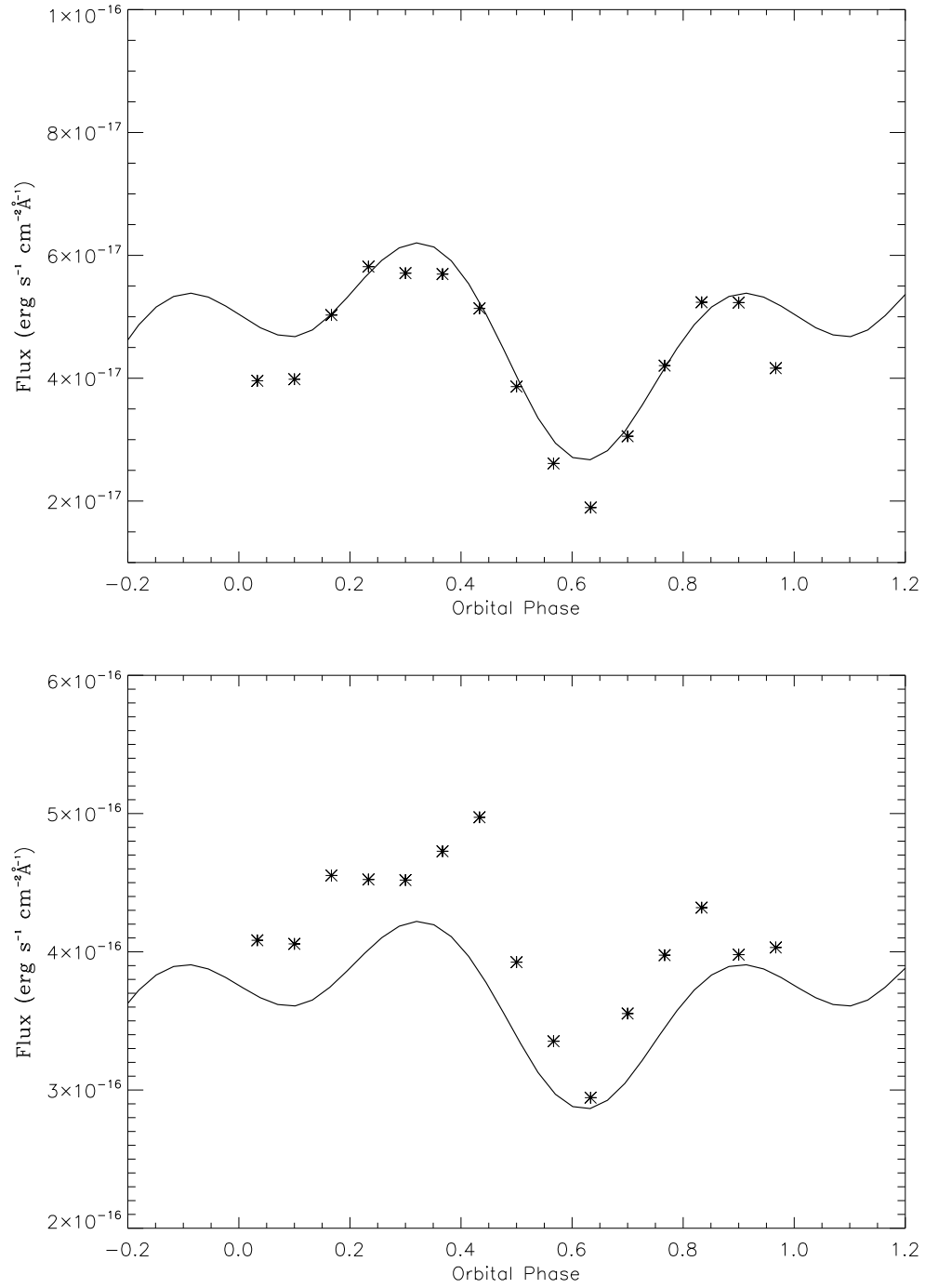


Fig. 4.— Synthetic photometry FUV (top) and NUV (bottom) light curves of WX LMi as seen from 107 pc. Note the different ordinate scales.

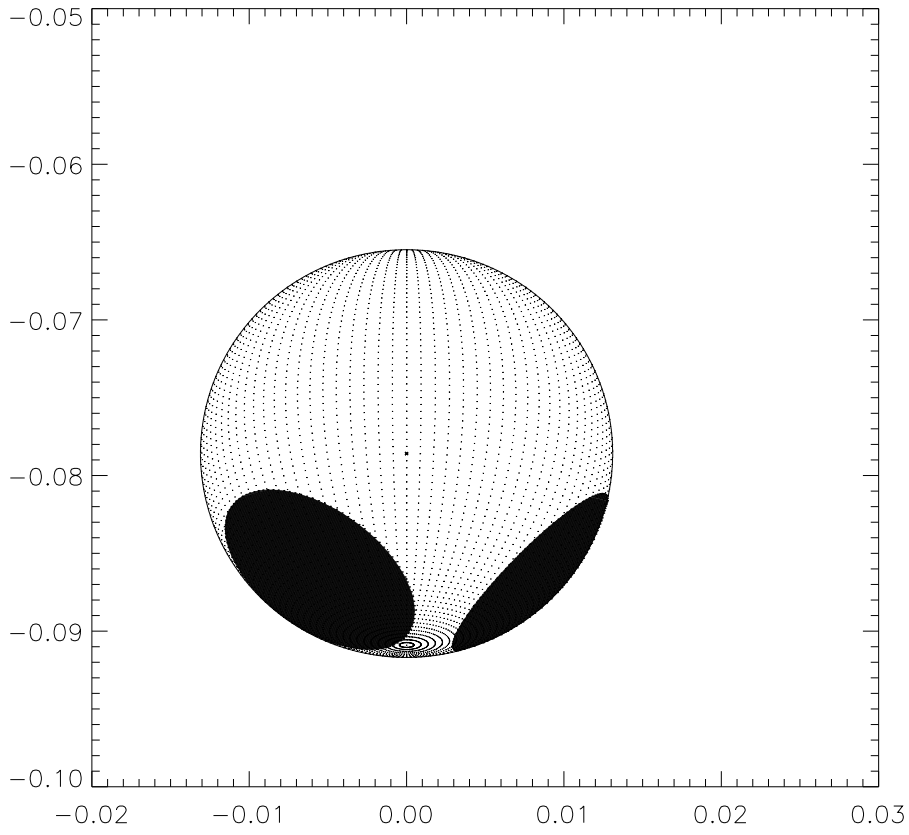


Fig. 5.— View of WX LMi white dwarf at orbital phase 0.0, showing the two photospheric hot spots. See text for discussion.



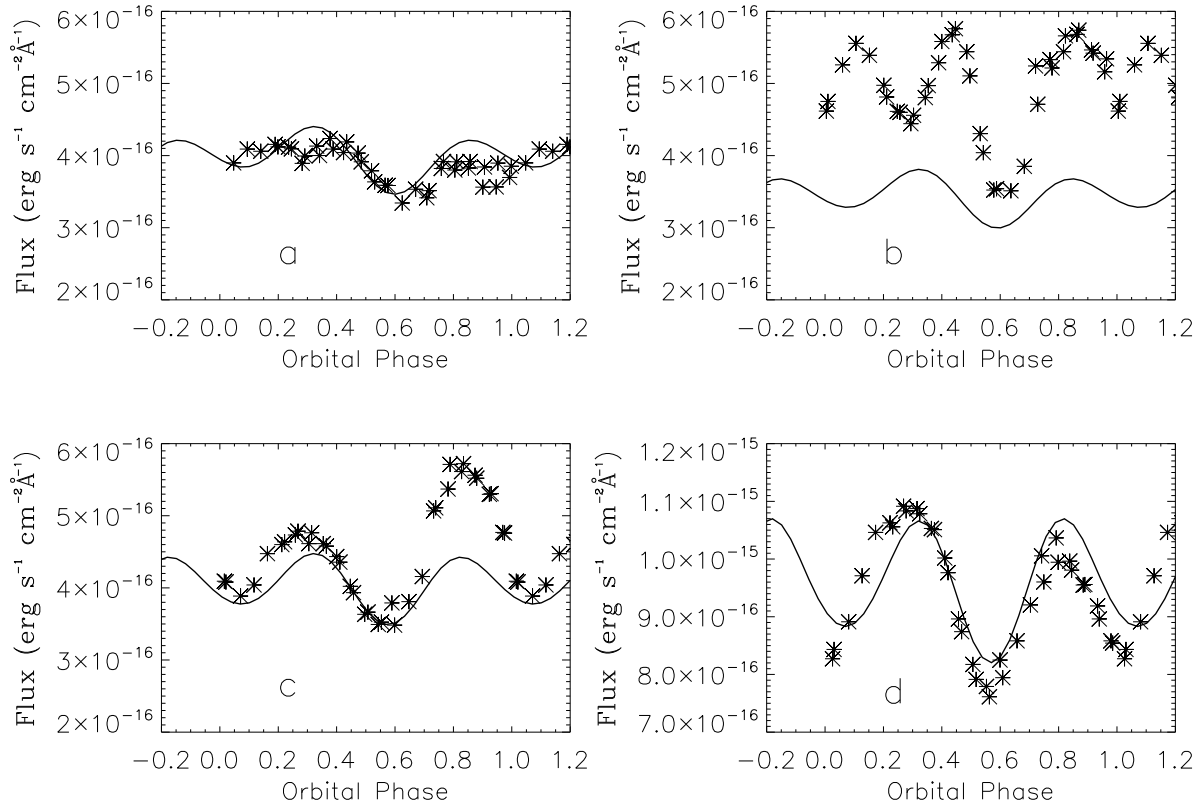


Fig. 6.— Synthetic light curves of WX LMi calculated with a secondary underfilling its volume by 90%; compare to Figure 3.

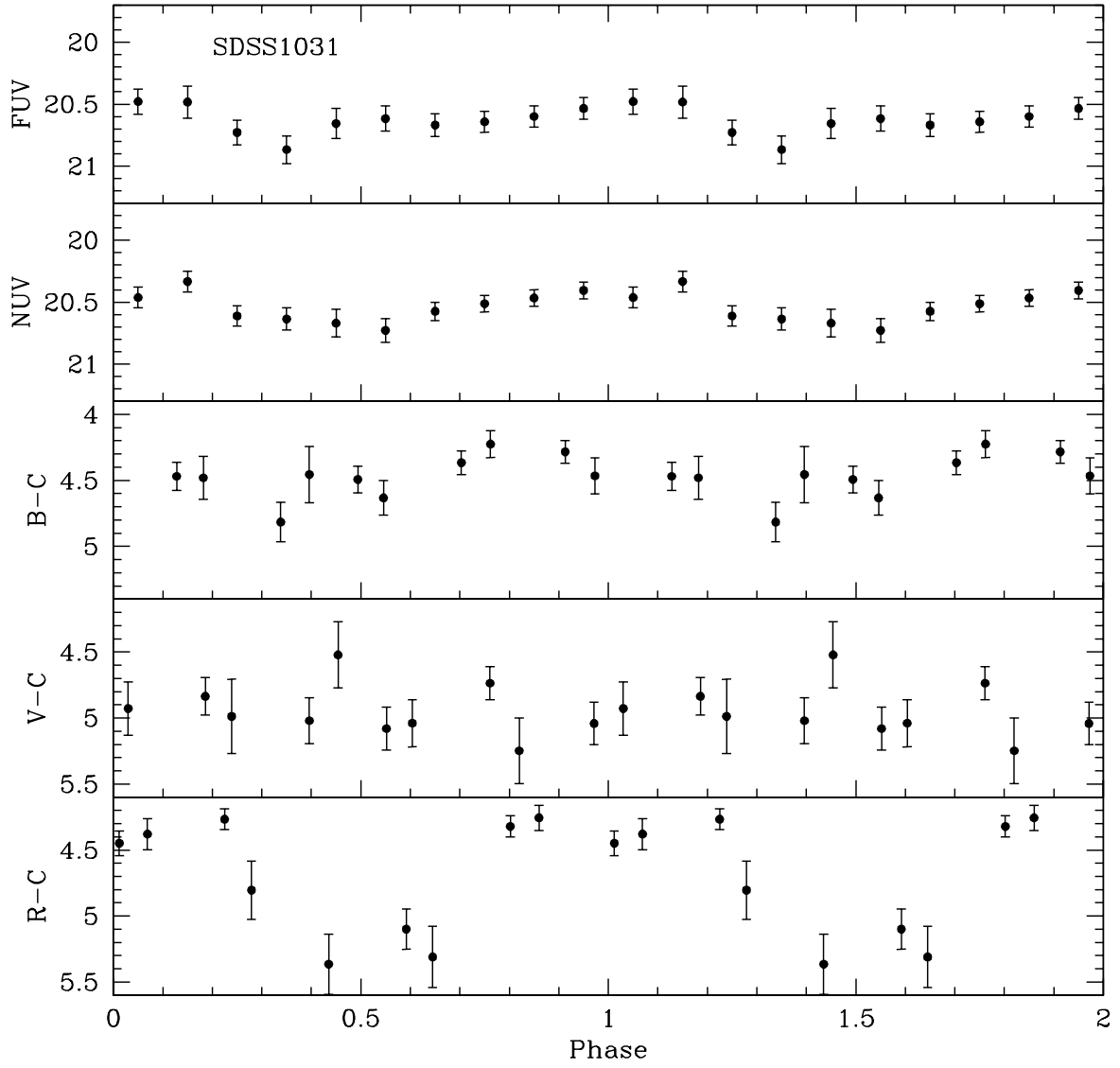


Fig. 7.— *GALEX* FUV and NUV and optical *B*, *V*, *R* filter light curves as a function of phase (phases are arbitrary) for SDSS1031. Light curves are repeated from phases 1.0 to 2.0.

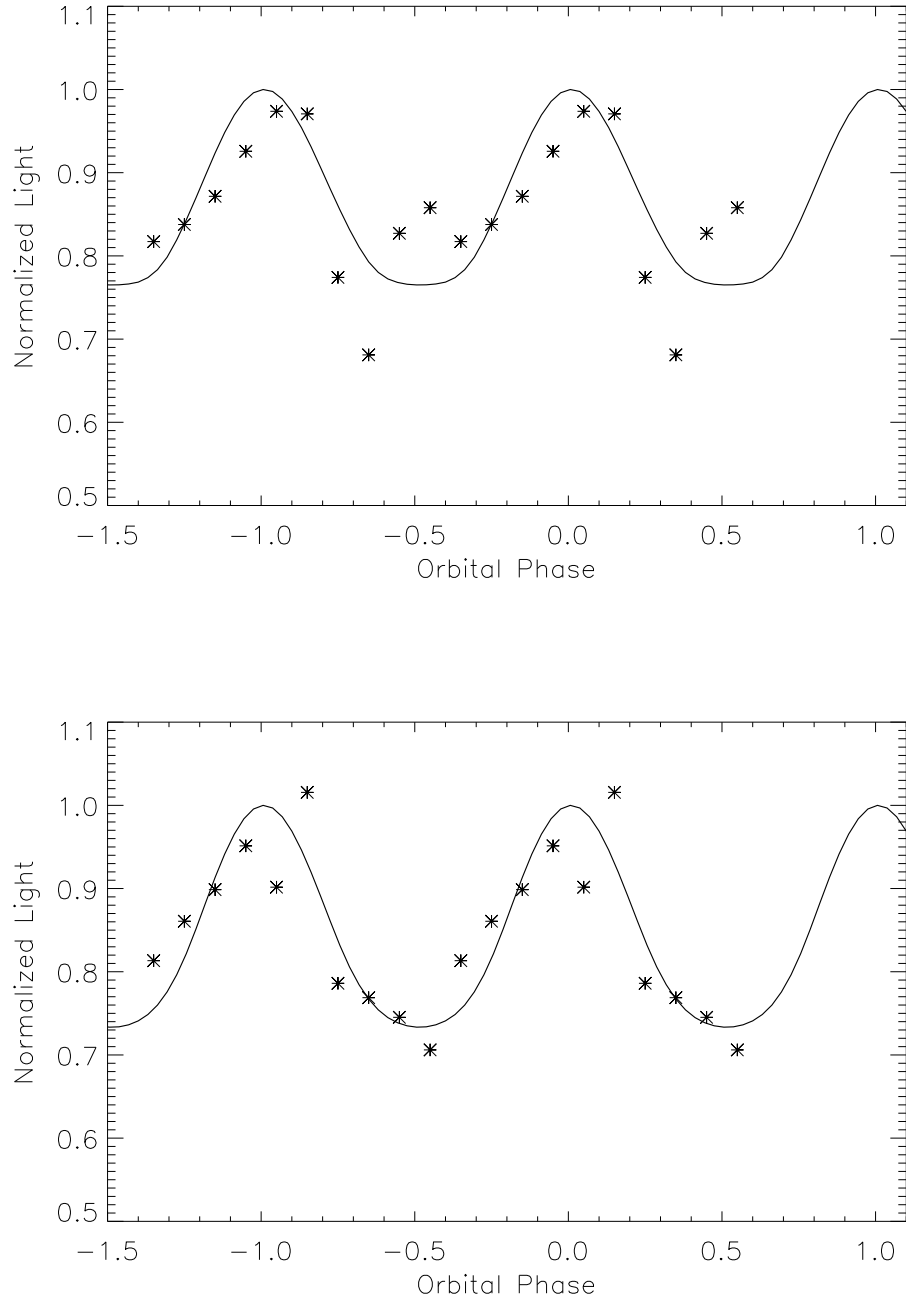


Fig. 8.— Spot Model fits from Table 4 for the *GALEX* FUV (top) and NUV (bottom) light curves of SDSS1031.

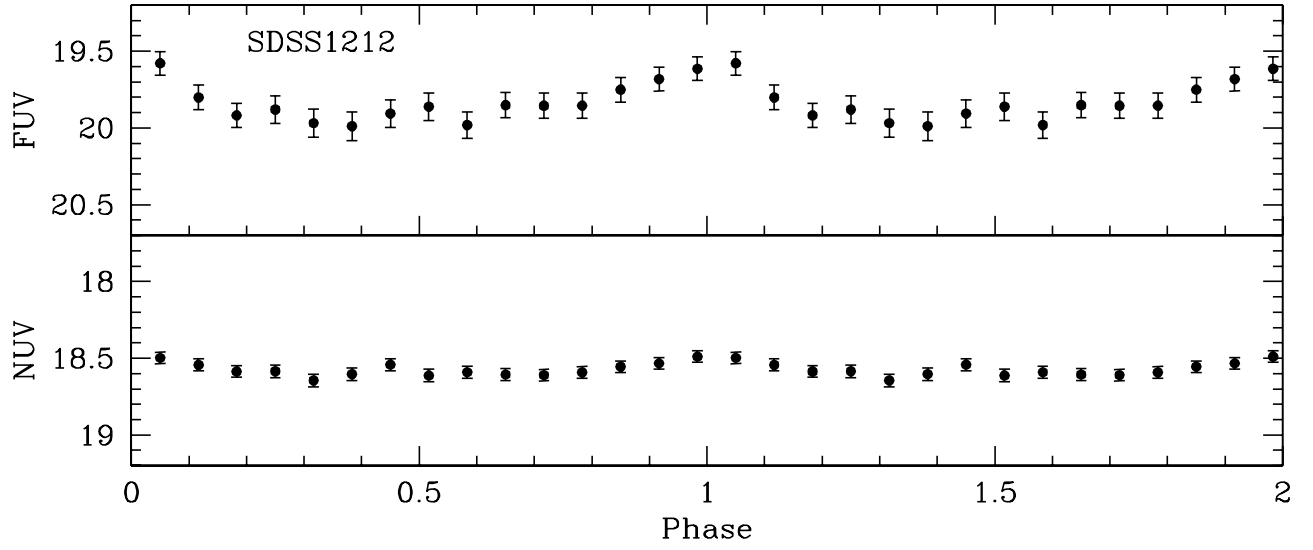


Fig. 9.— *GALEX* FUV and NUV light curves as a function of phase (phase 0 is optical photometric maximum with phasing from B06) for SDSS1212.

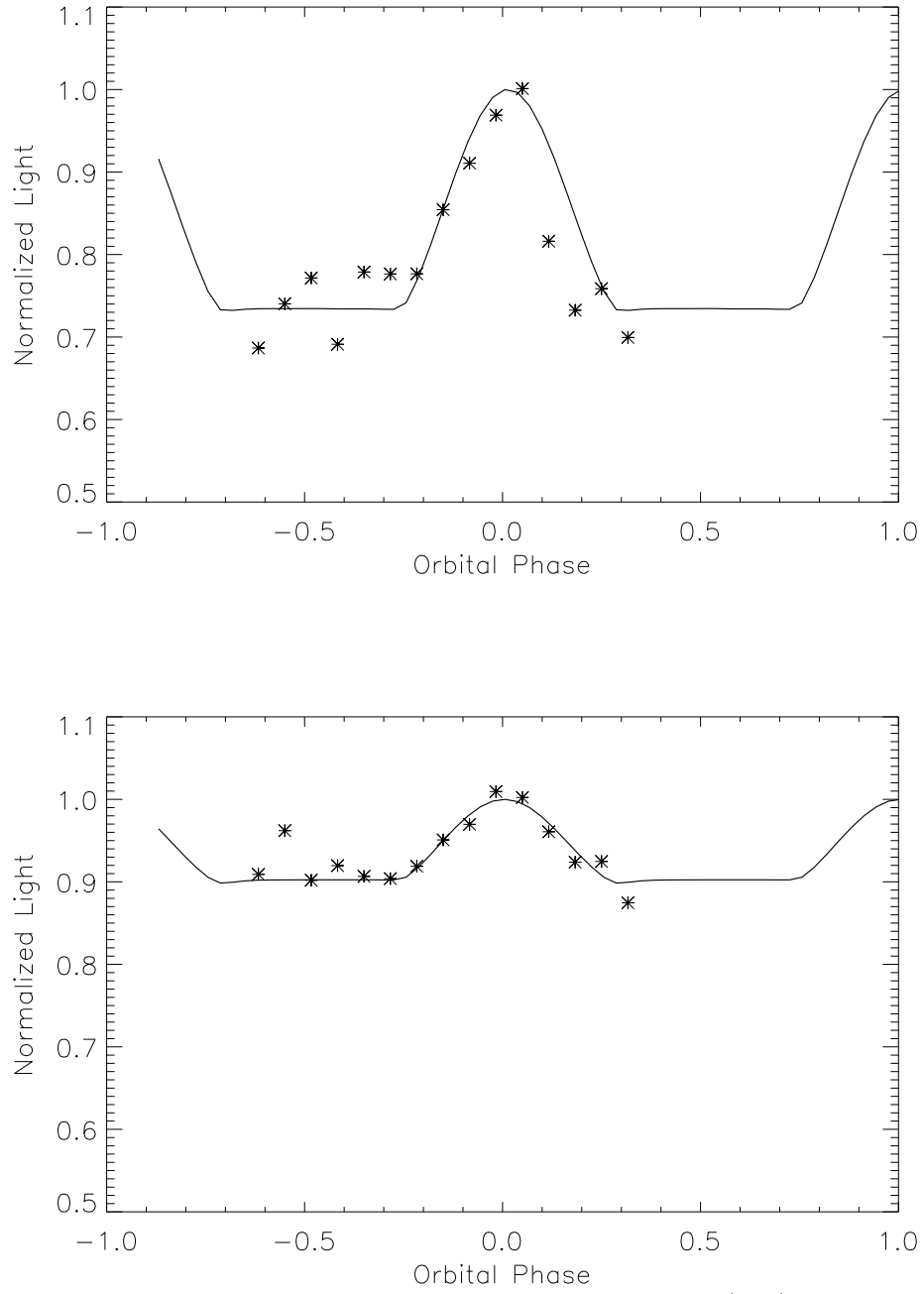


Fig. 10.— Spot Model fits from Table 4 for the *GALEX* FUV (top) and NUV (bottom) light curves of SDSS1212.